

Showcasing research from Dr Joshua Philip Barham's laboratory, Faculty of Chemistry and Pharmacy, University of Regensburg, Regensburg, Germany.

An organophotocatalytic late-stage N-CH₃ oxidation of trialkylamines to *N*-formamides with O₂ in continuous flow

Herein, a selective N-CH₃ to *N*-formyl late-stage functionalization of complex, bioactive alkaloids with molecular oxygen is enabled by organophotocatalysis and continuous flow microfluidic technology. A new dicyanoanthracene catalyst, accessible from cheap starting materials without chromatography, exhibited enhanced solubility for flow processing. Mechanistic studies revealed that the novel catalyst diverted the photochemical mechanism from electron transfer to energy transfer, increasing the efficiency of the reaction *via* a singlet oxygen sensitization pathway.

Image created by Sarah S. Coutts.

As featured in:



See Joshua P. Barham *et al.*, *Chem. Sci.*, 2022, **13**, 1912.

Cite this: *Chem. Sci.*, 2022, 13, 1912

All publication charges for this article have been paid for by the Royal Society of Chemistry

An organophotocatalytic late-stage N–CH₃ oxidation of trialkylamines to N-formamides with O₂ in continuous flow†

Mark John P. Mandigma,^a Jonas Žurauskas,^a Callum I. MacGregor,^b Lee J. Edwards,^b Ahmed Shahin,^{ac} Ludwig d'Heureuse,^a Philip Yip,^d David J. S. Birch,^d Thomas Gruber,^a Jörg Heilmann,^a Matthew P. John^b and Joshua P. Barham^{id* a}

We report an organophotocatalytic, N–CH₃-selective oxidation of trialkylamines in continuous flow. Based on the 9,10-dicyanoanthracene (DCA) core, a new catalyst (DCAS) was designed with solubilizing groups for flow processing. This allowed O₂ to be harnessed as a sustainable oxidant for late-stage photocatalytic N–CH₃ oxidations of complex natural products and active pharmaceutical ingredients bearing functional groups not tolerated by previous methods. The organophotocatalytic gas–liquid flow process affords cleaner reactions than in batch mode, in short residence times of 13.5 min and productivities of up to 0.65 g per day. Spectroscopic and computational mechanistic studies showed that catalyst derivatization not only enhanced solubility of the new catalyst compared to poorly-soluble DCA, but profoundly diverted the photocatalytic mechanism from singlet electron transfer (SET) reductive quenching with amines toward energy transfer (E_nT) with O₂.

Received 22nd October 2021
Accepted 26th December 2021

DOI: 10.1039/d1sc05840a

rsc.li/chemical-science

Introduction

A quintessential theme in medicinal chemistry is probing structure activity relationships. While strategies such as *de novo* and diversity-oriented synthesis are powerful tools to achieve this task, late-stage functionalization (LSF) has gained traction over the past decade as it offers a quicker route to access libraries of complex bioactive molecules from a defined core structure.^{1,2} Among the myriad of methods that are applied in LSF, C–H functionalization is undeniably an attractive and potent addition to a synthetic chemist's arsenal, given the ubiquity of C–H bonds in molecules.^{1–3} This umbrella term stretches over traditional transition metal catalysis to alkali and base-metal catalysis to organocatalysis and photocatalytically-enabled transformations. Recent examples demonstrate the value of C–H functionalization of simple and complex amides through ionic⁴ or radical⁵ mechanisms. Trialkylamines are especially important targets since they are well represented in

the alkaloids, a family of potent bioactive molecules that has shaped the natural sciences.^{6,7} N–CH₃ groups are attractive loci for C–H functionalization in pharmaceutical research, since incremental structural variations carry substantial pharmacological effects (Fig. 1), for example in bioactivities of opiates.⁸ However, C–H bonds α to N are relatively inert. Access to derivatives was historically carried out stepwise, leveraging the nucleophilicity of the N atom, usually requiring initial demethylations of trialkylamine N–CH₃ groups to free N–H secondary amines for subsequent transformations.⁹ That is until the renaissance of single electron transfer (SET) redox methods, partly driven by photoredox catalysis, which have revolutionized practices in organic synthesis.¹⁰ This allowed direct C–H functionalizations α to N, of benzylic amines with nucleophiles¹¹ and a few examples of aliphatic amines with electrophiles.¹² A direct and highly N–CH₃-selective LSF of trialkylamines was achieved using stoichiometric quantities of an SET-generated hydrogen atom transfer agent (DABCO⁺).¹³ Powerful catalytic

^aFakultät für Chemie und Pharmazie, Universität Regensburg, 93040 Regensburg, Germany. E-mail: Joshua-Philip.Barham@chemie.uni-regensburg.de

^bGlaxoSmithKline Medicines Research Centre, Gunnels Wood Road, Stevenage SG1 2NY, UK

^cChemistry Department, Faculty of Science, Benha University, 13518 Benha, Egypt

^dDepartment of Physics, SUPA, University of Strathclyde, 107 Rottenrow East, Glasgow, G4 0NG, UK

† Electronic supplementary information (ESI) available. CCDC 2109522. For ESI and crystallographic data in CIF or other electronic format see DOI: 10.1039/d1sc05840a

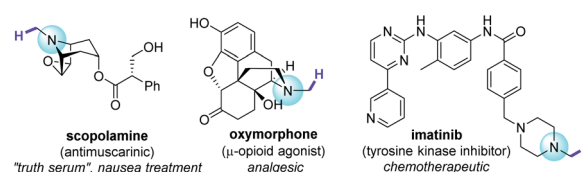


Fig. 1 Bioactive trialkylamines and target sites for N–CH₃ C–H functionalization.



or photocatalytic LSF strategies for complex trialkylamines have emerged, but remain scarce.¹⁴

Direct C–H oxidation of a trialkylamine's N–CH₃ group to an *N*-formyl group is a worthy endeavour as *N*-formamide products (and mechanisms to access them) are relevant to oxidative metabolite research,¹⁵ are natural products,^{6,16} and serve as synthetic handles¹⁷ for further modifications including Barbier-type amidations,¹⁸ C–C cross-couplings,¹⁹ amino-carbonylations of alkenes or alkynes,²⁰ and couplings with phenols²¹ or amines²² (affording carbamates or ureas, respectively). *N*-Formamides are classically accessed from trialkylamines by toxic Ru(IV) or Os(IV) oxidants (Fig. 2A).^{23–27}

Recently, Yamaguchi and co-workers circumvented this *via* an elegant Cu(II)/Cu(I) and nitroxyl radical catalyst system.²⁸ Song and co-workers reported a transition metal (T.M.)-free deconstructive formylation reaction.²⁹ The main drawbacks of such previous methods are (i) the incompatibility of redox-sensitive functionalities common to complex pharmaceuticals, hence limiting their application to relatively simple amines, and (ii) the expense of reagents (hindered nitroxyl radical catalysts^{28b} and excess difluorocarbene reagents) which are economically impractical for scale-up. We contemplated an alternative strategy using an organophotocatalyst, in order to avoid toxic, precious, unsustainable T.M.-based photocatalysts.³⁰ Simultaneously, and inspired by numerous reports of gas–liquid photocatalytic flow

processes,³¹ we envisaged that continuous flow would allow us to efficiently and safely handle O₂ as a simple, abundant, sustainable terminal oxidant. The rapid uptake of continuous flow reactors in the synthesis of fine materials and pharmaceuticals is worth noting, as is their innovative marriage with visible light irradiation which drastically enhanced the efficiency, sustainability and safety of photochemical processes.³² Previous organophotocatalytic activations of trialkylamines using O₂ were reported, but those instead targeted (i) *N*-demethylations of opiates and tropanoids,³³ (ii) endocyclic C–H cyanations α to N³⁴ or (iii) oxidations of benzylic amines.³⁵ We were particularly drawn to 9,10-dicyanoanthracene (DCA) as used by Santamaria and co-workers (Fig. 2B). Using DCA as a potent photooxidizing catalyst ($E_{1/2}[\text{DCA}^*/\text{DCA}^{\cdot-}] = +1.99 \text{ V vs. SCE}$),³⁰ air (O₂) as terminal oxidant, and an LiClO₄ additive, they reported variable amounts of *N*-formyl products (2) in batch, however *N*-demethylation (nor-amines (3)) competed or dominated reactions.^{36,37} Herein, we report a late-stage organophotocatalytic oxidation of N–CH₃ groups that selectively delivers *N*-formyl compounds (2). Our method leverages mild conditions and continuous flow processing to handle O₂ safely as a terminal oxidant (Fig. 2C). Key to the aforementioned achievements was the design of a novel dicyanoanthracene catalyst that not only enhanced solubility for flow processing, but switched the excited state mechanism from single electron transfer with amines toward energy transfer with O₂.

Results and discussion

Photocatalyst and process design

At the onset, our attempts to use DCA using modified reaction conditions of Santamaria in batch (and in flow) were severely obstructed by its poor solubility in MeCN (*i.e.*, turbidity and sedimentation were observed). The suspended, undissolved photocatalyst was detrimental to photochemistry due to hindering light penetration of the reaction. Furthermore, in continuous flow this often led to flow channel blockages and longer reaction times (for details, see ESI† file). Thus, design of a catalyst with enhanced solubility was required (Fig. 3).

Intuitively, introduction of polar substituents improves solubility of compounds in polar aprotic solvents. Nitro- and sulfonic acid- groups are good choices for polyaromatic compounds as the synthetic process to access them is straightforward. Glöckhofer and co-workers reported the synthesis of a dinitro derivative of DCA with improved solubility.³⁸ On the other hand, sulfonic acids carry the advantage of further derivatization *via* their sulfonyl chlorides. Inspired by intermediates reported in the synthesis of a water-soluble DCA analogue,³⁹ we began our catalyst synthesis (Fig. 3). Anthraquinone-2,6-disulfonic acid 4, commercially supplied or easily synthesized from cheap anthraquinone,⁴⁰ was reduced by activated Zn in aq. (NH₄)₂CO₃ to afford anthracene-2,6-disulfonic acid 5 in good (65%) yield after acidic workup and recrystallisation from aq. KCl. Electrophilic bromination of the central ring of 5 gave 6 in high (80%) yield. At this stage, our synthesis deviated from the literature cyanation which digested the crude product (containing CuCN) in conc. HNO₃ and

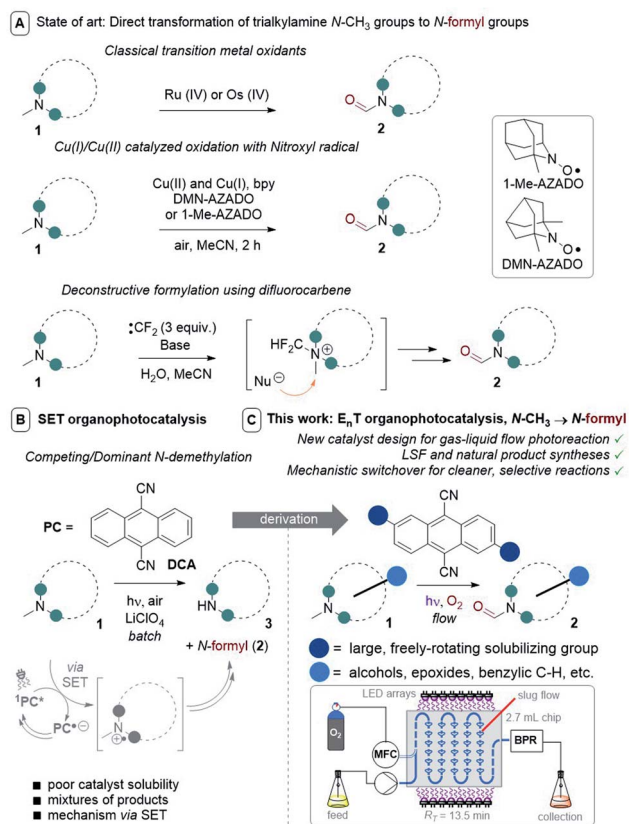


Fig. 2 Strategies for selective N–CH₃ to *N*-formyl oxidations. PC = photocatalyst, MFC = mass flow controller (O₂), BPR = back pressure regulator, R_T = retention time.



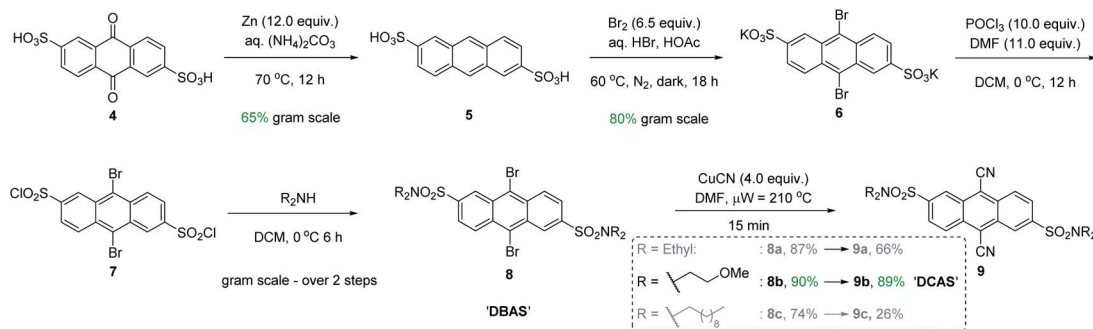


Fig. 3 Chromatography-free gram scale synthesis of DCAS photocatalyst.

liberated toxic HCN gas. However, both Rosenmund von-Braun and Pd-catalysed cyanations failed to cyanate **6** due to its poor solubility in organic solvents. Tohnai and co-workers had reported that the derivatization of anthraquinone disulfonic acids (ADS) as their organic ammonium salts (*i.e.*, *n*-heptyl and *n*-pentyl) prevented π -stacking interactions of ADS as observed by crystallography.^{41,42} Instead of ammonium salts which would hinder characterization and reaction workup, we achieved this covalently with sulfonamides.

Therefore, **6** was derivatized to increase its solubility in polar aprotic organic solvents and to increase prospects for successful cyanation. Chlorination of **6** with POCl₃ and subsequent trapping of **7** with secondary amines of various chain lengths gave 9,10-dibromoanthraquinone-2,6-disulfonamides (**DBAS**) **8a**, **8b** and **8c** in 87, 90 and 74% yields, respectively. Pleasingly, Rosenmund von-Braun cyanations under microwave-assisted (15 min) or thermal (see ESI[†]) heating afforded 9,10-dicyanoanthraquinone-2,6-disulfonamides **9a**, **9b** (**DCAS**) and **9c** as 'brilliant yellow' solids in 66%, 89% and 26% yields, respectively. We note that our entire synthesis to **9** is carried out on gram scale, with straightforward purification *via* recrystallisation instead of chromatography. Photocatalyst **9b** (henceforth coined '**DCAS**') was progressed to evaluation in reactions since it: (i) displayed the highest solubility in MeCN ($1.900 \pm 0.100 \text{ mg mL}^{-1}$ vs. $0.340 \pm 0.006 \text{ mg mL}^{-1}$ for **DCA**) consistent with its calculated physical property values (which showed that it was the least lipophilic and had the highest topological polar surface area, see ESI[†]),⁴³ and (ii) was obtained in the highest overall yield (42% over 5 steps).

Studies using a homogeneous liquid flow photoreactor

Next, **DCAS** was tested under some initial photocatalytic flow conditions (Table 1) in a commercial tubular coil continuous flow photoreactor (Vapourtec Ltd R-series/UV-150). Using **1a** (12 mM) as our substrate and 5 mol% of **DCAS** at rt, a maximum yield of 25% for **2a** (with 4 : 1 of **2a** : **3a** selectivity) was obtained under recycling conditions (90 min) no matter whether dry air, O₂, or (1 : 1) N₂/O₂ were used (entry 2). The absence of catalyst (entry 2) or O₂ led to no reaction. We found out that in the absence of LiClO₄, single pass conditions gave a similar yield (25%) and with much improved selectivity for **2a** (entry 4, **3a** was not detected). When the temperature was increased to 40 °C, the

yield improved to 40% (entry 5). Under similar conditions but employing **DCA** as catalyst afforded **2a** in 15% yield, confirming superiority of **DCAS** under flow conditions. A batch reaction mimicking Santamaria and co-workers' condition (entry 8) afforded a complex reaction mixture (see ESI[†]). Our previously reported batch anaerobic conditions for SET oxidation of *N*-alkyl tetrahydroisoquinolines with [Ru(bpy)₃]²⁺ photocatalysis^{11b} in batch (entry 7) gave no reaction, and when the more potent photooxidizing SET catalyst [Ru(bpz)₃]²⁺ was used only traces of **3a** were observed. As such and due to cost of the catalysts, we did not examine these any further in flow.

When under N₂ protection (entry 3), a purple coloration in the post-reactor flowing reaction mixture was observed (see ESI[†]) which hinted at formation of **DCAS**^{•−}. We note that the related parent structure **DCA**^{•−} is well-known to be purple in color.⁴⁴ When the purple post-reactor reaction mixture was collected and exposed to air, immediate discoloration back to yellow was observed. From these observations, we had initially assumed

Table 1 Initial photocatalyst screening for *N*-CH₃ to *N*-formyl oxidation of a trialkylamine

Entry	PC	Deviation from condition	2a : 3a ^a	% Yield of 2a ^a
1	DCAS	Dry air, O ₂ or N ₂ /O ₂ (1 : 1)	4 : 1	25
2	—	Dry air	n.r.	n.d.
3	DCAS	N ₂	n.r.	n.d.
4 ^b	DCAS	O ₂ , R _T = 20 min, no LiClO ₄	>30 : 1	25
5 ^{b,c}	DCAS	O ₂ , R _T = 20 min, no LiClO ₄	>30 : 1	40
6 ^{b,c}	DCA	O ₂ , R _T = 20 min, no LiClO ₄	>30 : 1	15
7 ^d	DCA	Batch, h ν > 420 nm	—	c.r.m.
8 ^d	[Ru] ^e	Batch, 459 nm	—	Traces 3a

^a Selectivity and yields determined by ¹H NMR of the crude reaction mixture using 1,3,5-trimethoxybenzene (TMB) as internal standard.

^b Single pass. ^c T = 40 °C. ^d For exact details of conditions including terminal oxidants attempted, see ESI. ^e 1 mol% of Ru(bpy)₃Cl₂ or Ru(bpz)₃(PF₆)₂. PC = photocatalyst, n.r. = no reaction, n.d. = not detected, c.r.m. = complex reaction mixture.



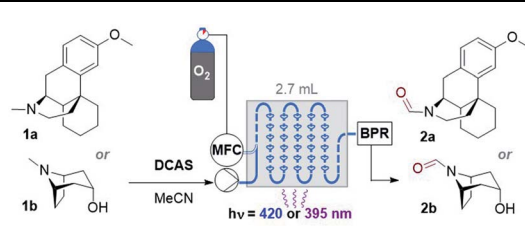
a reductive SET quenching of ¹DCAS* by the amine, as originally proposed by Santamaria and co-workers (Fig. 2B).^{36,37} However, this was later refuted (see the Mechanistic studies for details).

Based on this mechanistic assumption, we reasoned that formation of **2a** reached its upper limit due to limiting oxygen solubility at ambient conditions in the tubular reactor, preventing catalyst turnover. The solubility of O₂ in an O₂-saturated solution of MeCN is 8.1 mM,⁴⁵ and considering the theoretical requirement of 2 equiv. O₂ to remove 2 electrons from the trialkylamine, mass transfer limits full conversion of a reaction mixture containing 12.0 mM trialkylamine (later in the revised mechanism, we find that [O₂] is still a limiting factor for the reaction yield).

Studies using a gas–liquid flow photoreactor

Considering the abovementioned observations, we opted for a photoreactor designed for biphasic gas–liquid reactions. A commercial microfluidic continuous flow photoreactor (Corning Lab Photoreactor©) designed for excellent mixing *via* turbulent slug flow allowed us to safely operate up to 60 °C and 8 bar backpressures. The hazard of the flammable reaction mixture was safely contained by the thermal isolation of the flow path and the small volume of reaction mixture (2.7 mL) at any given time. A summary of reaction condition optimization is shown in Table 2 (see ESI† for full optimization). Transferring conditions from the previous tubular reactor (Table 1, entry 5), **2a** was afforded in 22% yield (Table 2, entry 1), as expected since the decreased yield exactly consists with (is proportional to) the decreased residence time (*R_T*). However, the yield almost doubled when 395 nm LEDs were used (entry 2), which accorded with a higher extinction coefficient of DCAS's UV-vis band at *ca.* 395 nm compared to its 420 nm band (*vide infra*). At 24 mM **1a** and double the residence time, the yield increased to 44% (entry 7). At 48 mM of **1a** the yield decreased to 24% (entry 8), presumably again due to the limiting [O₂]. At *T* = 60 °C and 24 mM **1a**, the yield of **2a** marginally improved to 46% (entry 9). The inherent back pressure on the flow by the microfluidic module was sufficient to ensure precise, reproducible, low flow rates (down to 0.1 mL min⁻¹) up to 60 °C. To our delight, tropane **1b** afforded **2b** in 60% under reaction conditions at *T* = 40 °C and *R_T* = 27 min (entry 10) despite its free 2° alcohol typically prone to oxidation under similar oxidative conditions.^{23–28,46} Decreasing catalyst loading decreased the yield (entries 11 and 12). Like the case of substrate **1a**, a marginal increase of yield to 61% occurred at 60 °C (entry 13). At this stage, we explored the effect of a back pressure (8 bar) to evaluate higher O₂ solubility (entries 14–16). At lower backpressures, the flow was heterogeneous slug flow but at 7–8 bar, homogenous flow was observed indicating full solubilization of O₂ and higher dissolved [O₂]. At 7–8 bar, doubling the concentration to 48 mM or using a residence time as short as *R_T* = 6.8 min negatively impacted the yield of **2b** (entries 14 and 15), but we found that yield (61%) was preserved at *R_T* = 13.5 min (entry 16 *vs.* 13). This doubled productivity of **2b** to 0.65 g per day which was the upper limit of the gas–liquid organophotocatalytic flow reaction in this system.

Table 2 Reaction optimization in a gas–liquid flow reactor^{ab}



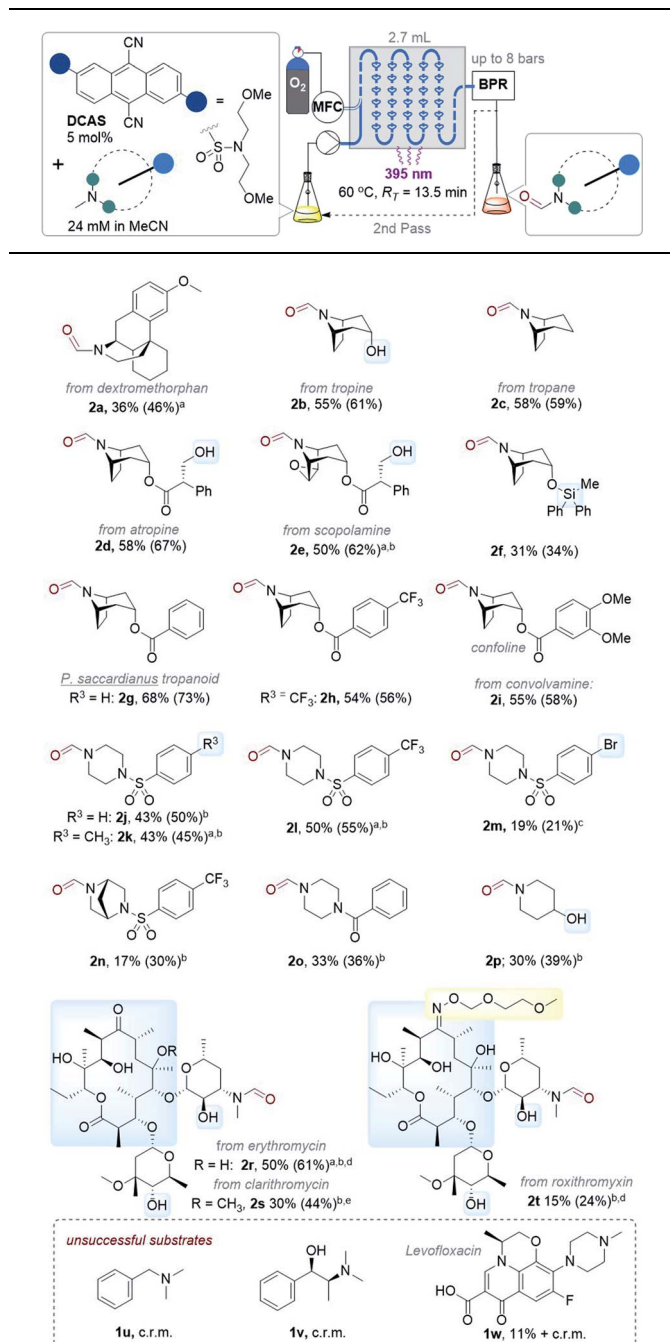
Entry	Amine	Conc. (mM)	<i>R_T</i> ^c (min)	<i>hν</i> (nm)	<i>T</i> (°C)	% Yield ^d
1	1a	12	13.5	420	40	22 (2a)
2	1a	12	13.5	395	40	40 (2a)
3	1a	12	5.4	395	40	12 (2a)
4	1a	12	~1.0	395	40	Trace (2a)
5	1a	12	~1.0	None	40	n.r.
6	1a	24	13.5	395	40	40 (2a)
7	1a	24	27.0	395	40	44 (2a)
8	1a	48	27.0	395	40	24 (2a)
9 ^e	1a	24	27.0	395	60	46 (2a)
10	1b	24	27.0	395	40	60 (2b)
11 ^f	1b	24	27.0	395	40	53 (2b)
12 ^g	1b	24	27.0	395	40	42 (2b)
13 ^e	1b	24	27.0	395	60	61 (2b)
14 ^{e,h}	1b	48	13.5	395	60	48 (2b)
15 ^{e,h}	1b	24	6.8	395	60	31 (2b)
16 ^{e,h}	1b	24	13.5	395	60	61 (2b)

^a Unless otherwise stated, reaction conditions: DCAS (5 mol%), O₂ (ambient pressure), at 40 °C. ^b *T* = 25 °C. ^c *R_T* = residence time = (2.7 mL)/(flow rate). ^d Yield determined by ¹H NMR using 1,3,5-TMB as internal standard. ^e *T* = 60 °C. ^f DCAS (3 mol%). ^g DCAS (1 mol%). ^h At 7–8 bar back pressure. MFC = mass flow controller (O₂), BPR = back pressure regulator, n.r. = no reaction.

Next, we tested the scope of the reaction (Table 3). Since isolations of polar formamides were oftentimes challenging due to the *N*-formyl group being a weak chromophore, the following discussion deems ¹H NMR yields more representative of reaction efficiency. Compounds **2c** (59%) and **2d** (67%) were obtained from natural products tropane and (free alcohol-bearing) atropine. Even scopolamine, which has a free alcohol, an ester, and an epoxide, afforded **2e** in 62% yield with no nor-scopolamine detected, albeit requiring 2 passes through the reactor (total *R_T* = 27 min). This contrasts with Santamaria and co-workers' conditions using DCA and without LiClO₄, which afforded a 1 : 1 mixture of **2e** : nor-scopolamine.^{36,37} Compared to **2b**, the yield of **2f** was lower (34%) presumably due to the presence of the Si protecting group known to stabilize radicals and quench excited photosensitizers *via* different pathways.⁴⁷ Benzoyl-containing compound **2g** was afforded in good (73%) yield. Electron-poor (-CF₃) and electron-rich (-OMe) substituents on the benzoyl group were tolerated equally, affording **2h** (56%) and **2i** (58%) respectively. We note both **2g** and **2i** are natural products; novel tropanoid compound **2g** was recently isolated from *Pellacalyx saccardianus* and our method corroborated its proposed structure.⁴⁸ Compound **2g** (confoline) was isolated from *Convolvulus subhirsutus* and our method accessed it from convolvamine in a single step (in the literature, semi-



Table 3 Scope of organophotocatalytic flow N-CH₃ to *N*-formyl oxidation



^a $R_T = 27$ min, O₂ (ambient pressure). ^b 2 passes. ^c 12 h recycling. ^d 12 mM. ^e 6 mM. Yields in parenthesis determined by ¹H NMR of the reaction mixture using 1,3,5-TMB as internal standard. c.r.m. = complex reaction mixture.

synthesis of **2i** was achieved by formylation of norconvolvamine, hence a demethylation step from convolvamine culminates in a two-step process).¹⁷ Compounds **2j** to **2o** were obtained from piperazines as common API fragments (such as those present in sildenafil and danofloxacin).⁴⁹ Despite having 3

possible sites for functionalization (one exocyclic N-CH₃ and two endocyclic N-CH₂-R sites), selective oxidation at the N-CH₃ (*exo*:*endo* = 5.7:1 for **2j**, 3.4:1 for **2k**, 3.7:1 for **2l**, and 6.5:1 for **2p**, see ESI†) was apparent, affording *N*-formyl compounds in respectable yields. Despite the modest yields of products **2l** (55%), **2m** (21%), and **2n** (30%) (as well as **2h**), we were surprised by the tolerance of halogen-bearing substrates under the reaction conditions. Especially, given the aforementioned putative presence of DCAS^{•-} *via* reductive quenching of ¹DCAS* by trialkylamines (well known for DCA's case)^{50,51} and given that photoexcited radical anions are known to reductively cleave aryl halides and other strong bonds.⁵⁰⁻⁵³ C-F bonds and N-Ts groups are also prone to reductive cleavage under reductive photocatalysis⁵⁴ or by photoexcited super electron donors.⁵⁵

A simple piperidine **2p** (39%) was also tolerated. Our success with **2b**, **2d**, **2e**, and **2p** whose precursors bore free alcohol groups encouraged us to explore more complex molecules. Gratifyingly, conditions were successfully applied to macrolide antibiotics with dense functionalities (free alcohols, an oxime ether, and a ketone). Erythromycin, clarithromycin and roxithromycin afforded **2r**, **2s**, and **2t** in 61%, 44%, and 24% yields, respectively. However, benzylic amines and trialkylamines containing benzylic alcohols or free carboxylic acids such as **1u**, **1v** and **1w**, were unsuccessful. Benzaldehyde formation (C-N cleavage, possibly *via* endocyclic iminium ion formation and then hydrolysis) and intractable complex reaction mixtures were observed for these substrates.

Mechanistic studies

Cyclic voltammetry (CV) revealed DCAS ($E_{1/2}[\text{DCAS}/\text{DCAS}^{\bullet-}] = -0.59$ V vs. SCE) is substantially easier to reduce than DCA ($E_{1/2}[\text{DCA}/\text{DCA}^{\bullet-}] = -0.98$ V vs. SCE), due to the electron-withdrawing sulfonamide groups at the 2,6-positions (Fig. 4, left). UV-vis absorption and emission spectra were measured for DCA and DCAS (Fig. 4, right) and their comparison revealed that the 2,6-sulfonamides hardly affect the absorptive or emissive profiles of the dicyanoanthracene core. In both cases, overlap of the longest wavelength absorption band ($\lambda_{\text{max}} = 422$ nm) and shortest wavelength emission band ($\lambda_{\text{max}} = 435$ nm) allows to approximate E^{0-0} for the singlet excited state (≈ 2.90 eV). Taking this value together with measured redox potentials, the photocatalyst excited state oxidation potentials were approximated by

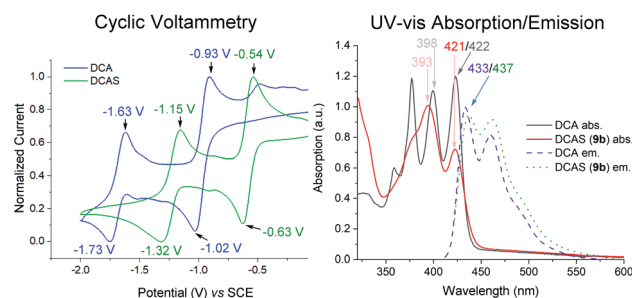


Fig. 4 Left: cyclic voltammetry of catalysts. Conditions: 0.01 M DCA/DCAS in 0.1 M ⁿBu₄NPF₆/MeCN, scan rate 50 mV s⁻¹. Right: UV-vis and emission spectra.



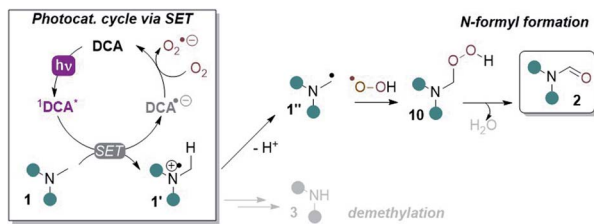


Fig. 5 SET reductive quenching mechanism of DCA proposed by Santamaria and co-workers leading to demethylation and *N*-formyl products.

a derivative of the Rehm–Weller equation.⁵⁶ $^1\text{DCAS}^*$ ($E_{1/2}[^1\text{DCAS}^*/\text{DCAS}^{\bullet-}] = +2.31 \text{ V vs. SCE}$) is a notably more potent photooxidant than $^1\text{DCA}^*$ ($E_{1/2}[^1\text{DCA}^*/\text{DCA}^{\bullet-}] = +1.93 \text{ V vs. SCE}$). Our initial hypothesis thus continued to align with the SET mechanism proposed by Santamaria (Fig. 5).^{36,37} In this premise, $^1\text{DCAS}^*$ was assumed to behave like $^1\text{DCA}^*$ which underwent reductive quenching by trialkylamine **1**, and oxidation of $\text{DCAS}^{\bullet-}$ by O_2 regenerated DCAS . Deprotonation of radical cation $1^{\bullet+}$ and radical combination of the α -amino radical and superoxide would ultimately afford *N*-formyl product **2**. We note SET reactions were also proposed as the main pathways for trialkylamine activations by thiazine and fluorescein organophotocatalysts, either *via* oxidation to *N*-oxides or *via* *N*-demethylations.⁵⁷

To test this initial hypothesis, two control batch experiments with stoichiometric (2.0 equiv.) DCA and DCAS were conducted under strict N_2 protection in PhCN solvent to promote solubility. Both afforded clean conversion of **1a** to a 1 : 1 mixture of **1a** : **3a** (Fig. 6A), although DCA 's reaction required $>3.5\times$ reaction time due to poorer solubility. Upon irradiation, the reaction mixtures changed from a pale yellow color to dark purple (Fig. 6B). Removal the light and exposing to air, the colors of reaction solutions quickly reverted to yellow (consistent with aforementioned observations of the flow reaction under N_2). The UV-vis spectra of $\text{DCA}^{\bullet-}$ is well studied in the literature,^{51,53} and it is known to be purple in color.⁴⁴ We confirmed the presence of $\text{DCAS}^{\bullet-}$ spectroscopically by matching the spectra of a sample of DCAS treated by cathodic electrolysis to that treated photochemically in the presence of a trialkylamine reductive quencher (see ESI† for details). Both gave a new, broad absorption spectrum at the visible-green region ($\lambda_{\text{max}} \approx 544 \text{ nm}$, Fig. 6C), thus an apparent purple color.

A Time-Dependent Density Functional Theory (TD-DFT) calculation of the UV-vis transitions of $\text{DCAS}^{\bullet-}$ consisted with this green absorption peak ($\lambda_{\text{max}} = 547 \text{ nm}$). The detection of these radical anions together with *N*-demethylation reaction confirmed that the SET oxidation of **1** to $1^{\bullet+}$ by the organophotocatalysts was possible, at least under anaerobic conditions. Considering the preceding discussion supportive of an SET mechanism in Fig. 5 and catalysts' redox potentials, one would expect $^1\text{DCAS}^*$ to undergo more rapid fluorescence quenching than $^1\text{DCA}^*$ by trialkylamines. Very surprisingly, the opposite was clearly true (Fig. 7). The Stern–Volmer rate constant for quenching of $^1\text{DCAS}^*$ by **1a** ($k_{\text{q}} = 1.44 \times 10^9 \text{ M}^{-1} \text{ s}^{-1}$) was two orders of magnitude smaller than that of $^1\text{DCA}^*$ (k_{q}

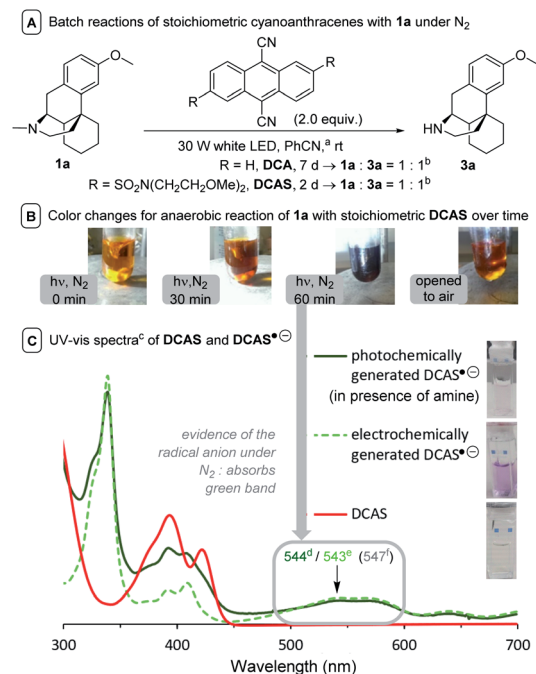


Fig. 6 Experiments suggesting the generation of cyanoanthracene radical anions. (A) ^aDue to stoichiometric PC loadings, PhCN was chosen as solvent for improved solubility. ^bIn the absence of additional base, **1a** deprotonates $1a^{\bullet+}$ to afford $1a^{\bullet-}$, meaning the reaction fundamentally could never exceed 50% conversion. (B) Observed color changes. (C) ^cIn MeCN, λ_{max} at the visible region when ^dgenerated by photochemical reductive quenching of $^1\text{DCAS}^*$ with a trialkylamine; ^egenerated electrochemically; or ^fcalculated using TD-DFT at CAM-B3LYP/6-31++g(2d,p), CPCM(MeCN) level of theory (for details, see ESI†).

$= 1.69 \times 10^{11} \text{ M}^{-1} \text{ s}^{-1}$).^{58,59} Presumably, either (i) the 2-methoxyethyl groups of DCAS affects the kinetics of bimolecular quenching by sterically obstructing the approach of trialkylamine, or (ii) aggregation of DCA accelerates reductive quenching by trialkylamines⁶⁰ where DCAS exhibits a different kind of aggregation in solution.⁶¹

To probe the mechanistic role of the structural changes on the catalyst, and to rationalize the unexpected trend between the order of redox potentials of $^1\text{DCA}^*$ and $^1\text{DCAS}^*$ vs. their fluorescence quenching rates, DFT and TD-DFT calculations were performed. The activation energies ($\Delta G_{\text{SET}}^\ddagger$) for the

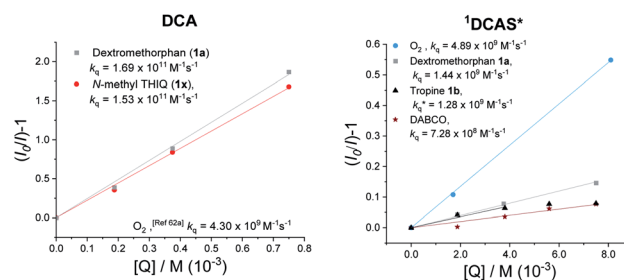
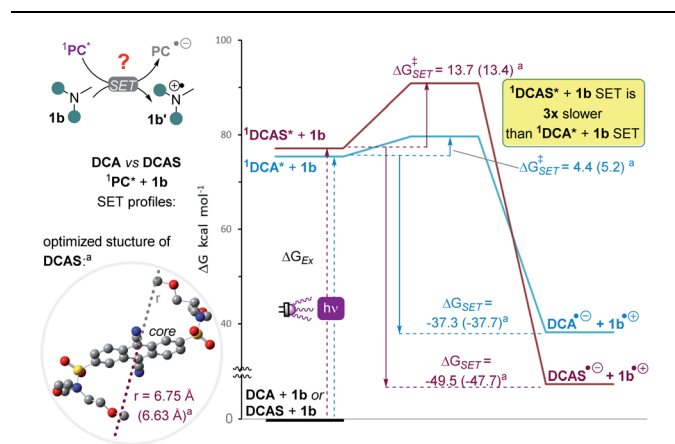


Fig. 7 Stern–Volmer quenching experiments of DCA (right) and DCAS (left) with various amine quenchers (under N_2) or O_2 .

photoinduced single electron transfer (SET) from **1b** to photoexcited dicyanoanthracenes were determined using Marcus theory (Table 4). Aside from free energy (ΔG_{SET}), another key parameter of Marcus theory is the reorganization energy (λ) which accounts for the properties of the solvent, the size of, and the distance between reacting species. The calculated vertical excitation energies ($\Delta G_{\text{Ex}} \approx 3.3$ eV) were close to E^{0-0} value obtained from optical spectroscopy (*vide supra*). As expected from the experimentally-determined photocatalyst redox potentials, SET of **1b** with $^1\text{DCAS}^*$ is $1.3\times$ more exergonic ($\Delta G_{\text{SET}} = -49.9$ kcal mol $^{-1}$) than with $^1\text{DCA}^*$ ($\Delta G_{\text{SET}} = -37.3$ kcal mol $^{-1}$). However, the kinetic barrier is notably ($3\times$) higher for $^1\text{DCAS}^*$ ($\Delta G_{\text{SET}}^\ddagger = 13.7$ kcal mol $^{-1}$) than $^1\text{DCA}^*$ ($\Delta G_{\text{SET}}^\ddagger = 4.4$ kcal mol $^{-1}$). This agreed with the relatively slower fluorescence quenching of $^1\text{DCAS}^*$ by trialkylamines. However, this is juxtaposed with the greater synthetic efficiency of the reaction catalysed by **DCAS** compared to **DCA**. Taken together, these results show that although SET between excited cyanoanthracenes and trialkylamines can occur under anaerobic conditions, an alternative mechanism must operate for **DCAS** under aerobic conditions in order for it to deliver higher synthetic efficiencies.

Elsewhere, $^1\text{DCA}^*$ is also known as an efficient singlet oxygen sensitizer ($k_q = 4.3 \times 10^9$ M $^{-1}$ s $^{-1}$) *via* a photosensitized energy transfer (E_{nT}) mechanism.⁶² The high reported quantum yield (reaching 2.0) supports the generation of $2 \times ^1\text{O}_2$ molecules per $1 \times ^1\text{DCA}^*$.⁶² This quenching rate constant of $^1\text{DCA}^*$ by E_{nT} is

Table 4 Calculated kinetics and thermodynamics for photoinduced SET of $^1\text{PC}^*$ s with **1b**^a



$^1\text{PC}^*$	k_q^b	ΔG_{Ex}^c	ΔG_{SET}^d	$\Delta G_{\text{SET}}^\ddagger^e$
DCA	1.69×10^{11}	75.4 (75.9)	-37.3 (-37.7)	4.4 (5.2)
DCAS	1.44×10^9	77.2 (76.8)	-49.9 (-47.7)	13.7 (13.4)
DCAS/DCA	~ 0.01	~ 1 (~ 1)	1.3 (1.3)	3.1 (2.6)

^a Geometry optimization, molecular radius (r) and free energies calculated using DFT (ground state) or TD-DFT (excited state) at CAM-B3LYP (or $\omega\text{B97X-D}$ in parentheses)/6-31+g(2d,p), CPCM(acetonitrile) level of theory (see ESI). ^b From Stern-Volmer analyses (Fig. 7), in M $^{-1}$ s $^{-1}$. ^c Vertical excitation energy. ^d Photoinduced-SET free energy. ^e Photoinduced-SET activation energy. All free energy units in kcal mol $^{-1}$. PC = photocatalyst. For further details, see ESI.

more than double that of the reductive SET quenching of $^1\text{DCAS}^*$ by trialkylamines. Thus, as $[\text{O}_2]$ increases and approaches that of the trialkylamine ($[\text{O}_2] \approx [\text{trialkylamine}]$), singlet oxygen generation dominates in the case of $^1\text{DCAS}^*$. This consists with the increase in yields observed at higher back pressures, temperatures and thus higher dissolved $[\text{O}_2]$. The k_q for quenching of $^1\text{DCAS}^*$ by O_2 was slightly higher (4.89×10^9 M $^{-1}$ s $^{-1}$ Fig. 7, left) than that reported for $^1\text{DCA}^*$.^{62a} Taken together with the fluorescence quenching rates (k_q) with trialkylamines, this points to a photochemical mechanistic switchover: $^1\text{DCA}^*$ is quenched faster ($39\times$) by **1a** than O_2 , while $^1\text{DCAS}^*$ is quenched faster ($3\times$) by O_2 than **1a**. Thus, under aerobic reaction conditions, $^1\text{DCA}^*$ favors an SET mechanism while $^1\text{DCAS}^*$ favors an E_{nT} mechanism.

We then studied the behaviour of the excited cyanoanthracenes under the aerobic reaction conditions (*i.e.*, catalyst, trialkylamine and O_2 (from air) are all present). This was done by comparing the relative intensity change of light (420 nm) transmitted through the coil of the tubular flow reactor. The principle is as follows: the faster the excited state catalyst can relax to the ground state, the greater the steady-state population of ground state photocatalyst is, leading to more absorption of light (therefore less transmission). The aerated, flowing reaction mixture of **DCA** (5 mol%) + **1a** (12 mM), under the conditions of Table 1, entry 6, gave minimal light absorption (Fig. 8A). As discussed earlier, the reductive quenching of $^1\text{DCA}^*$ by **1a** is even faster than quenching by O_2 and does not directly afford **DCA** but affords $\text{DCA}^{\cdot-}$ whose absorption^{51,53} is shifted far into the visible green region and thus is not detected by the probe. Regeneration of the ground-state catalyst relies on the oxidation of $\text{DCA}^{\cdot-}$ by O_2 , which is comparatively slow. In the absence of **1a**, the aerated solution of **DCA** (Fig. 8B) gave strong light absorption (decrease of transmitted light intensity to roughly half). O_2 no longer competes with **1a** and is now the exclusive

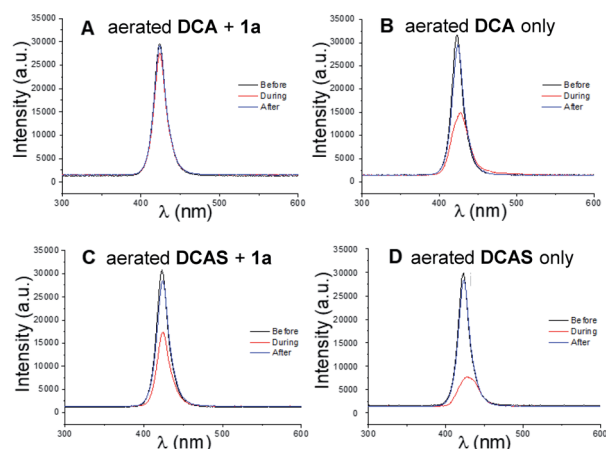


Fig. 8 Transmission intensity of light through the tubular reactor. (A) **DCA** (5 mol%) + **1a** (12 mM) in aerated MeCN; (B) **DCA** only in aerated MeCN; (C) **DCAS** (5 mol%) + **1a** (12 mM) in aerated MeCN; (D) **DCAS** only in MeCN. Before/After = light transmission before or after the reaction mixture passed through the tubular coil reactor, *i.e.* flowing MeCN only. During = light transmission while the reaction mixture slug is flowing through the coil and upon reaching a steady value.

quencher, regenerating and sustaining a large steady-state concentration of absorbing **DCA** via rapid E_nT quenching of $^1\text{DCA}^*$. In contrast, the reaction mixture (Table 1, entry 4) of **DCAS** (5 mol%) in MeCN gave notable light absorption even when **1a** (12 mM) was present (Fig. 8C), since quenching of $^1\text{DCAS}^*$ by O_2 now outcompetes reductive quenching by **1a**, ensuring a larger steady-state concentration of absorbing **DCAS**. This agrees with the aforementioned differences in quenching rate constants. Finally, the light absorption of an aerated solution of **DCAS** in the absence of **1a** (Fig. 8D) was greater in the absence of competing **1a**, and was more pronounced than in the case of **DCA** (Fig. 8B). This reflects the enhanced fluorescence quenching of the former with O_2 (for light transmission measurements under N_2 or with 380 nm, see ESI†).

The lifetimes of $^1\text{DCA}^*$ and $^1\text{DCAS}^*$ as measured by Time-correlated Single Photon Counting (TSCPC) in MeCN under Ar were similar, at 14.5 and 13.8 ns, respectively (Table 5).

The lifetime of $^1\text{DCA}^*$ was 1.8 ns lower in presence of air, while the lifetime of $^1\text{DCAS}^*$ was 4.7 ns lower, confirming the slight enhancement of quenching by O_2 (and consistent with the Stern–Volmer k_q s of $^1\text{DCAS}^*$ and $^1\text{DCA}^*$, *vide supra*). Further experiments supported the photosensitized E_nT quenching of $^1\text{DCAS}^*$ as the dominant mechanism, rather than photoinduced SET to afford $\text{O}_2^{\cdot-}$ (Fig. 9A and B). Firstly, when α -terpinene was employed as the substrate, ascaridole was formed in 65% yield as quantified by ^1H NMR. Endoperoxide formation is a hallmark reporter for $^1\text{O}_2$ through its Diels–Alder [4 + 2]-cycloaddition with dienes (Fig. 9A, left),⁶³ thus confirming $^1\text{DCAS}^*$ is capable of $^1\text{O}_2$ generation. Secondly, the presence of DABCO as an additive inhibited conversion in **1b**'s reaction (Fig. 9B, right). Despite DABCO's low oxidation potential ($E_{\text{ox}}^{\text{p}} = +0.66$ V),¹³ this inhibition was not due to its competitive SET reductive quenching of $^1\text{DCAS}^*$, since the quenching rate constant ($k_q = 7.28 \times 10^8 \text{ M}^{-1} \text{ s}^{-1}$) confirmed it was even less efficient as a quencher of $^1\text{DCAS}^*$ than O_2 or **1a/1b** (Fig. 7). Rather, DABCO is a well-known physical quencher of $^1\text{O}_2$.^{64,65} This was confirmed by a linear correlation ($R^2 = 0.997$) between the reciprocal relative rate and [DABCO], an experiment designed by Lapi and co-workers. Finally, as proof of the direct fixation of oxygen atoms from O_2 gas into trialkylamines, ^{18}O -**2b** was detected by HRMS when isotopically-enriched oxygen ($^{18}\text{O}_2$) gas was employed in the batch reaction of **1b** (Fig. 9B).

In summary, increased efficiency of **DCAS** over **DCA** in the reaction is not only attributed to the former's enhanced solubility. The sulfonamide substituents at the 2,6-positions of the

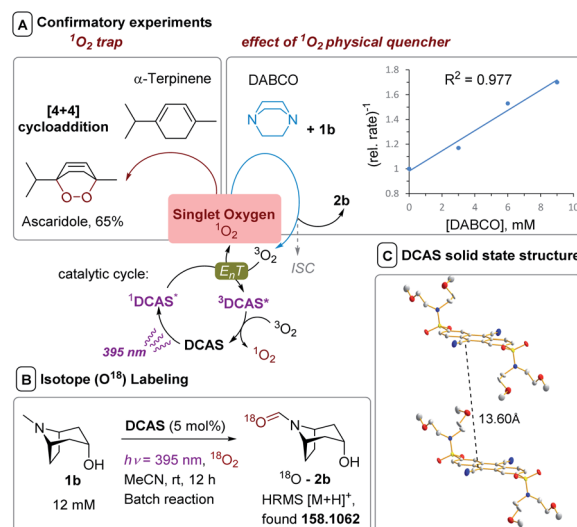


Fig. 9 Experiments evidencing (i) an $^1\text{O}_2$ mechanism, (ii) fixation of oxygen atoms from O_2 and (iii) breakup of π -stacking for **DCAS**. (A) Left: $^1\text{O}_2$ trapping via [4 + 2] cycloaddition. Reaction conditions: α -terpinene (12 mM), **DCAS** (5 mol%), O_2 (8 bar), $R_T = 13.5$ min, $h\nu = 395$ nm; right: effect of increasing [DABCO] on the (relative rate) $^{-1}$ of N-CH_3 **1b** oxidation. Reaction conditions: **1b** (12 mM), DABCO (0 to 9 mM), **DCAS** (5 mol%), O_2 (8 bar), $R_T = 13.5$ min, $h\nu = 395$ nm. Relative rate = (yield of **2b**)/(yield of **2b** with DABCO). (B) Isotope labeling batch reaction with $^{18}\text{O}_2$ gas. (C) XRD crystal structure of 2 molecules of **DCAS** with the distance between the anthracene cores. Thermal ellipsoids are set at the 50% probability level. H atoms are omitted for clarity, C atoms (grey), N atoms (blue), O atoms (red) S atoms (yellow).

dicyanoanthracene markedly decrease the reductive quenching of $^1\text{DCAS}^*$ by trialkylamines, compared to that of $^1\text{DCA}^*$. This observation may be explained by a change in the aggregation state of the organophotocatalyst,⁶¹ where the ordered π -stacking of **DCA** aggregates creates a large effective volume for collisions with amines, while **DCAS** behaves differently. The distance of π -sandwich planes for **DCA** = 3.37 Å and the usual range for 2 interacting planes is 3.3 to 3.8 Å.⁶⁶ In the X-ray diffraction (XRD) structure of **DCAS** (Fig. 9C), the distance between π -planes of anthracene = 13.60 Å and considering that $2r =$ distance between molecules, this value agrees with $2 \times$ the calculated spherical radii of **DCAS** in MeCN (Table 4). From this, we tentatively propose that the bulky, freely-rotating sulfonamide substituents sterically inhibit bimolecular (or unimolecular)⁵⁹ quenching events with trialkylamines. The smaller O_2 molecules outcompete larger trialkylamines to reach the cyanoanthracene core, diverting the mechanism to $^1\text{O}_2$ sensitization. This consists with the need for constrained trialkylamine substrates with protruding N-CH_3 groups herein, and may rationalize DABCO's inefficiency as a reductive quencher on steric grounds.¹³ A similar "steric-bulk" strategy was recently employed using *tert*-butyl substituents to prevent an unproductive EDA complexation in a catalytic reaction.⁶⁷

In light of all the above, we propose the following mechanism (Fig. 10). Photoexcitation of **DCAS** affords $^1\text{DCAS}^*$ which undergoes E_nT with $^3\text{O}_2$. The generated $^1\text{O}_2$ interacts with the trialkylamine via a well-studied exciplex,^{62,64,68,69} which can

Table 5 TSCPC-determined lifetimes of dicyanoanthracene catalysts under Ar vs. under air^a

Entry	Excited state PC	Sample preparation	t (ns)
1	DCA	Ar bubbling, 5 min	14.5 (14.9) ^b
2	DCA	Equilibrated in air	12.7 (12.6) ^b
3	DCAS	Ar bubbling, 5 min	13.8
4	DCAS	Equilibrated in air	9.1

^a See ESI for experimental details of TSCPC. ^b Literature values.



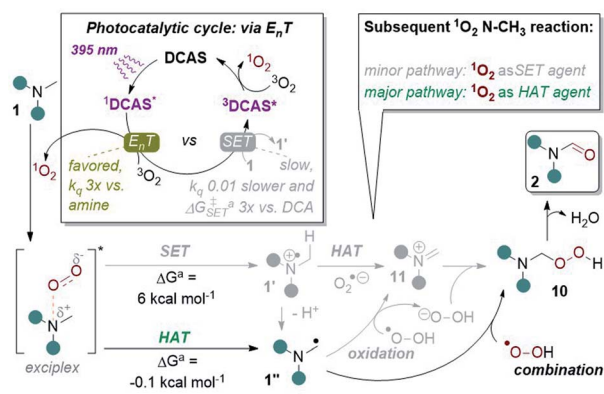


Fig. 10 Proposed reaction mechanism with key experimental and computational evidence. ^aDFT calculations at CAM-B3LYP/6-31++g(2d,p), CPCMC(acetonitrile) level of theory.

undergo one of two pathways: SET or HAT. Redox potentials dictate SET between trialkylamines ($E_{\text{ox}}^{\text{P}} > +0.9$ V vs. SCE)¹³ and $^1\text{O}_2$ ($E_{\text{red}}^{\text{P}} > +0.1$ V vs. SCE)⁶⁸ is endergonic, consistent with our DFT calculations of an endergonic free energy ($\Delta G = 6.0$ kcal mol⁻¹). Thus, we deemed SET within the exciplex as the minor pathway. Conversely, HAT within the exciplex was slightly exergonic ($\Delta G = -0.1$ kcal mol⁻¹) suggesting this is the major pathway. Combination of $1''$ with proximally-generated peroxy radical affords 10 (which could also be accessed by SET oxidation of α -amino radical $1''$ by $^1\text{O}_2$ followed by combination of 11 with $\text{O}_2^{\cdot-}$ and subsequent protonation is also possible). Finally, liberation of H₂O from 10 and DCAS is regenerated by the reported triplet-triplet annihilation of $^3\text{DCAS}^*$ with a second molecule of $^3\text{O}_2$.⁶²

In a recent study by Rovis, Schoenebeck and co-workers on the photocatalytic functionalizations of cyclic trialkylamines,^{14c} they proposed that a reversible and fast HAT is responsible for their endocyclic selectivity. Our computational studies point to a rapid, irreversible HAT in the $^1\text{O}_2$ -trialkylamine exciplex, thus steric factors must govern the selectivity (*i.e.* at the less sterically demanding N-CH₃ position). In the case of less-constrained trialkylamines (**1u**, **1v**), the $^1\text{O}_2$ -bound exciplex can react promiscuously in HAT with endocyclic/non-N-CH₃ positions (*e.g.* benzylic groups, free alcohols) leading overall to degradation.

Conclusions

Herein, we report DCAS as a new organophotocatalyst for late-stage N-CH₃ to *N*-formyl oxidations of complex trialkylamine-containing natural products and pharmaceuticals, using molecular oxygen and continuous flow. Redox sensitive functionalities were tolerated, allowing the LSF post-modification of alkaloids and macrolide antibiotics to their *N*-formyl derivatives in good yields with excellent chemo- and regioselectivities, all in a continuous manner. The safe handling of O₂ under increased back pressures and temperatures *via* gas-liquid continuous flow in turn promoted mass transfer of O₂ to the reaction, increasing yields, shortening reaction (residence) times to

several minutes and unleashing synthetically useful productivities (0.65 g per day). Mechanistic insights demonstrate how seemingly minor structural variations in an organophotocatalyst can not only increase solubility, but profoundly divert the excited state mechanism from photoinduced SET to E_nT, followed by a downstream HAT mechanism. Precious metal photocatalysts of Ru- and Ir-based polypyridyl complexes are well known to participate in both E_nT and SET, where structural tuning of ligands can affect switching between the divergent pathways. To our knowledge, such a concept has rarely been exploited in organophotocatalysis on the same core, privileged organophotocatalyst structures are typically developed either for SET or E_nT pathways. Switching the mechanism offers opportunities to control selectivity, as indicated by the tolerance of reductively-labile groups herein. With the generation of $^1\text{O}_2$ revealed, our study showcases one of few successful applications of $^1\text{O}_2$ as a reagent in complex natural product synthesis.^{31c,70} Further investigations on the selectivity of $^1\text{O}_2$'s reactions with trialkylamines and the nature of interactions between DCAS, O₂ and trialkylamine quenchers are ongoing.⁷¹

Data availability

Respectfully, all experimental and computational data is adequately available and retrievable from the ESI file.†

Author contributions

M. J. P. M. contributed the major effort on the optimization of the organophotocatalytic reaction in flow (microfluidic reactor), synthesized substrates, synthesized and purified all products and performed experimental mechanistic studies and computation; J. Ž developed an efficient synthetic route to new catalyst DCAS and synthesized gram quantities for the study; C. I. M. contributed preliminary studies on the optimization of the organophotocatalytic reaction in flow (tubular reactor); L. J. E. supervised and guided J. P. B. and C. I. M. in preliminary studies, measured light source emissions and transmission spectroscopy; A. S. undertook Stern-Volmer quenching studies and measured UV-vis spectroscopy of radical anion catalyst forms; L. d'H. contributed to the synthesis of complex trialkylamine substrates. P. Y. measured catalyst lifetimes and steady state emission spectroscopy. D. J. S. B. supervised and guided P. Y.; T. G. contributed to the separation of highly polar products by preparative HPLC; J. H. supervised and guided T. G.; M. P. J. supervised and guided J. P. B. in preliminary studies; J. P. B. conceptualized the project, conducted first investigations of photocatalytic trialkylamine activations, first synthesized new catalyst DCAS, measured cyclic voltammetry and UV-vis spectroscopy, guided and supervised C. I. M., M. J. P. M., J. Ž, A. S. and L. d'H. in their contributions.

Conflicts of interest

There are no conflicts to declare.



Acknowledgements

M. J. P. M., J. Ž., A. S., L. d'H. and J. P. B. thank the Alexander von Humboldt Foundation, within the framework of a Sofja Kovačevska Award endowed by the German Federal Ministry of Education and Research, for funding the main investigation. C. I. M., L. J. E., M. P. J. and J. P. B. thank GlaxoSmithKline for funding preliminary investigations. P. Y. and D. J. S. B. thank the Scottish Funding Council for a SUPA INSPIRE research studentship. The authors thank Prof. Dr Robert Wolf's group for access to a Glovebox; Katrin Kuck and Mirjam Abu Salah for technical assistance on preparative HPLC; Prof. Dr Oliver Reiser's group and Dr Christian Fischer for providing the resources to generate $^{18}\text{O}_2$ gas; and Prof. Dr Julia Rehbein for advice on DFT computations. We thank Regina Hoheisel for support in online irradiation/UV-vis measurements. The authors thank Philippe M. C. Roth and Marc Winter (Corning) for technical support. This paper is dedicated to the memory of Matthew P. John.

Notes and references

- M. Moir, J. J. Danon, T. A. Reekie and M. Kassiou, *Expert Opin. Drug Discovery*, 2019, **14**, 1137–1149.
- G. Wu, T. Zhao, D. Kang, J. Zhang, Y. Song, V. Namasivayam, J. Kongsted, C. Pannecouque, E. D. Clercq, V. Poongavanam, X. Liu and P. Zhan, *J. Med. Chem.*, 2019, **62**, 9375–9414.
- (a) L. Guillemard, N. Kaplaneris, L. Ackermann and M. J. Johansson, *Nat. Rev. Chem.*, 2021, **5**, 522–545; (b) T. Cernak, K. D. Dykstra, S. Tyagarajan, P. Vachal and S. W. Krska, *Chem. Soc. Rev.*, 2016, **45**, 546–576; (c) H. M. L. Davies and D. Morton, *J. Org. Chem.*, 2016, **81**, 343–350.
- (a) J. P. Barham, S. Tamaoki, H. Egami, N. Ohneda, T. Okamoto, H. Odajima and Y. Hamashima, *Org. Biomol. Chem.*, 2018, **16**, 7568–7573; (b) J. P. Barham, T. N. J. Fouquet and Y. Norikane, *Org. Biomol. Chem.*, 2020, **18**, 2063–2075; (c) M. J. P. Mandigma, M. Domański and J. P. Barham, *Org. Biomol. Chem.*, 2020, **18**, 7697–7723.
- (a) J. Kim, J. A. Ashenurst and M. Movassaghi, *Science*, 2009, **324**, 238–241; (b) J. Kaur, A. Shahin and J. P. Barham, *Org. Lett.*, 2021, **23**, 2002–2006; (c) J. Kim and M. Movassaghi, *Acc. Chem. Res.*, 2015, **48**, 1159–1171; (d) S. Das, K. Murugesan, G. J. V. Rodríguez, J. Kaur, J. P. Barham, A. Savateev, M. Antonietti and B. König, *ACS Catal.*, 2021, **11**, 1593–1603; (e) B. S. Bhakuni, A. Yadav, S. Kumar, S. Patel, S. Sharma and S. Kumar, *J. Org. Chem.*, 2014, **79**, 2944–2954.
- K. L. Kohnen-Johannsen and O. Kayser, *Molecules*, 2019, **24**, 796.
- (a) P. Le Couteur and J. Bureson, *Napoleon's buttons. 17 molecules that changed history*, Penguin, New York, 2004; (b) *Macrolide antibiotics: chemistry, biology, and practice*, ed. S. Omura, Academic Press, Amsterdam, Boston, 2nd edn, 2002; (c) *Dextromethorphan: pharmacology, clinical uses and health effects*, ed. X. Wang, Nova Biomedical, New York, 2016; (d) WHO, *Annex 1 19th WHO Model List of Essential Medicines*, WHO, Geneva, Switzerland, 2015.
- (a) A. P. Feinberg, I. Creese and S. H. Snyder, *Proc. Natl. Acad. Sci. U. S. A.*, 1976, **73**, 4215–4219; (b) M. Spetea and H. Schmidhammer, *Curr. Med. Chem.*, 2012, **19**, 2442–2457; (c) T. Kaserer, A. Lantero, H. Schmidhammer, M. Spetea and D. Schuster, *Sci. Rep.*, 2016, **6**, 1–15; (d) E. Prommer, *Support. Care Cancer*, 2006, **14**, 109–115; (e) T. R. Deer, M. S. Leong, A. Buvanendran, V. Gordin, P. S. Kim, S. J. Panchal and A. L. Ray, *Comprehensive Treatment of Chronic Pain by Medical, Interventional, and Integrative Approaches*, Springer, New York, 1st edn, 2013.
- (a) Z. Dong and P. J. Scammells, *J. Org. Chem.*, 2007, **72**, 9881–9885; (b) G. B. Kok, C. C. Pye, R. D. Singer and P. J. Scammells, *J. Org. Chem.*, 2010, **75**, 4806–4811; (c) A. Mary, D. Z. Renko, C. Guillou and C. Thal, *Tetrahedron Lett.*, 1997, **38**, 5151–5152; (d) K. McCamley, J. A. Ripper, R. D. Singer and P. J. Scammells, *J. Org. Chem.*, 2003, **68**, 9847–9850; (e) R. A. Olofson, R. C. Schnur, L. Bunes and J. P. Pepe, *Tetrahedron Lett.*, 1977, **18**, 1567–1570; (f) L. Werner, A. Machara, D. R. Adams, D. P. Cox and T. Hudlicky, *J. Org. Chem.*, 2011, **76**, 4628–4634; (g) W. Shu, A. Genoux, Z. Li and C. Nevado, *Angew. Chem., Int. Ed.*, 2017, **56**, 10521–10524.
- C. R. J. Stephenson and T. P. Yoon, *Visible light photocatalysis in organic chemistry*, Wiley-VCH, Weinheim, 1st edn, 2018.
- Selected examples: (a) G. Bergonzini, C. S. Schindler, C. J. Wallentin, E. N. Jacobsen and C. R. J. Stephenson, *Chem. Sci.*, 2013, **5**, 112–116; (b) J. P. Barham, M. P. John and J. A. Murphy, *Beilstein J. Org. Chem.*, 2014, **10**, 2981–2988; for a representative review, see: (c) J. W. Beatty and C. R. J. Stephenson, *Acc. Chem. Res.*, 2015, **48**, 1474–1484.
- (a) A. S. H. Ryder, W. B. Cunningham, G. Ballantyne, T. Mules, A. G. Kinsella, J. Turner-Dore, C. M. Alder, L. J. Edwards, B. S. J. McKay, M. N. Grayson and A. J. Cresswell, *Angew. Chem., Int. Ed.*, 2020, **59**, 14986–14991; (b) H. E. Askey, J. D. Grayson, J. D. Tibbetts, J. C. Turner-Dore, J. M. Holmes, G. Kociok-Kohn, G. L. Wrigley and A. J. Cresswell, *J. Am. Chem. Soc.*, 2021, **143**, 15936–15945; (c) J. H. Blackwell, G. R. Harris, M. A. Smith and M. J. Gaunt, *J. Am. Chem. Soc.*, 2021, **143**, 15946–15959.
- J. P. Barham, M. P. John and J. A. Murphy, *J. Am. Chem. Soc.*, 2016, **138**, 15482–15487.
- (a) J. He, L. G. Hamann, H. M. L. Davies and R. E. J. Beckwith, *Nat. Commun.*, 2015, **6**, 1–9; (b) J. Xie, S. Shi, T. Zhang, N. Mehrkens, M. Rudolph and A. S. K. Hashmi, *Angew. Chem., Int. Ed.*, 2015, **54**, 6046–6050; (c) T. Ide, J. P. Barham, M. Fujita, Y. Kawato, H. Egami and Y. Hamashima, *Chem. Sci.*, 2018, **9**, 8453–8460; (d) Y. Shen and T. Rovis, *J. Am. Chem. Soc.*, 2021, **143**, 16364–16369; (e) Y. Shen, I. Funez-Ardoiz, F. Schoenebeck and T. Rovis, *J. Am. Chem. Soc.*, 2021, **143**, 18952–18959.; for a review, see: (f) J. Kaur and J. P. Barham, *Synthesis*, 2021, DOI: 10.1055/a-1677-6619.
- (a) W. Ahmad, M. Z. Rehan, A. Gupta and J. Iqbal, *J. Saudi Chem. Soc.*, 2016, **20**, 543–546; (b) C. Köppel and



- J. Tenczer, *Biomed. Mass Spectrom.*, 1985, **12**, 499–501; (c) R. E. McMahon, H. W. Culp and J. C. Occolowitz, *J. Am. Chem. Soc.*, 1969, **91**, 3389–3390.
- 16 (a) N. A. Razzakov and S. F. Aripova, *Chem. Nat. Compd.*, 2004, **40**, 54–55; (b) E. G. Sharova, S. F. Aripova and S. Y. Yunusov, *Chem. Nat. Compd.*, 1980, **16**, 487–490; (c) *Natural compounds: plant sources, structure and properties*, ed. S. S. Azimova, Springer, New York, confoline, 2013; (d) H. Z. Zhang, Y. F. Wang, M. L. Zhang, M. Dong, C. H. Huo, F. Sauriol, Q. W. Shi, Y. C. Gu and H. L. Wang, *Chem. Nat. Compd.*, 2013, **48**, 1035–1038.
- 17 In contrast to secondary amines which provide nucleophilic activity, *N*-formamides react as electrophiles.
- 18 M. A. Ganiek, M. R. Becker, G. Berionni, H. Zipse and P. Knochel, *Chem.–Eur. J.*, 2017, **23**, 10280–10284.
- 19 S. Ding and N. Jiao, *Angew. Chem., Int. Ed.*, 2012, **124**, 9360–9371.
- 20 Y. Nakao, H. Idei, K. S. Kanyiva and T. Hiyama, *J. Am. Chem. Soc.*, 2009, **131**, 5070–5071.
- 21 N. V. Reddy, G. S. Kumar, P. S. Kumar, M. L. Kantam and K. R. Reddy, *Synlett*, 2014, **25**, 2133–2138.
- 22 G. S. Kumar, R. A. Kumar, P. S. Kumar, N. V. Reddy, K. V. Kumar, M. L. Kantam, S. Prabhakar and K. R. Reddy, *Chem. Commun.*, 2013, **49**, 6686–6688.
- 23 L. M. Berkowitz and P. N. Rylander, *J. Am. Chem. Soc.*, 1958, **80**, 6682–6684.
- 24 T. Endo and J. Zemlicka, *J. Org. Chem.*, 1979, **44**, 3652–3656.
- 25 S. W. Pelletier, H. K. Desai, J. Finer-Moore and N. V. Mody, *Tetrahedron Lett.*, 1982, **23**, 4229–4232.
- 26 R. Perrone, G. Carbonara and V. Tortorella, *Arch. Pharm.*, 1984, **317**, 635–639.
- 27 R. Perrone, G. Carbonara and V. Tortorella, *Arch. Pharm.*, 1984, **317**, 21–27.
- 28 (a) S. Nakai, T. Yatabe, K. Suzuki, Y. Sasano, Y. Iwabuchi, J. Y. Hasegawa, N. Mizuno and K. Yamaguchi, *Angew. Chem., Int. Ed.*, 2019, **58**, 16651–16659; (b) For comments on the cost comparisons of nitroxyl radical catalysts and DCAS, see ESI file.
- 29 J. Su, X. Ma, Z. Ou and Q. Song, *ACS Cent. Sci.*, 2020, **6**, 1819–1826.
- 30 N. A. Romero and D. A. Nicewicz, *Chem. Rev.*, 2016, **116**, 10075–10166.
- 31 (a) H. Seo, M. H. Katcher and T. F. Jamison, *Nat. Chem.*, 2017, **9**, 453–456; (b) N. Emmanuel, P. Bianchi, J. Legros and J. C. M. Monbaliu, *Green Chem.*, 2020, **22**, 4105–4115; (c) Z. Amara, J. F. B. Bellamy, R. Horvath, S. J. Miller, A. Beeby, A. Burgard, K. Rossen, M. Poliakoff and M. W. George, *Nat. Chem.*, 2015, **7**, 489–495; (d) S. Mazzanti, G. Manfredi, A. J. Barker, M. Antonietti, A. Savateev and P. Giusto, *ACS Catal.*, 2021, **11**, 11109–11116; (e) G. Laudadio, Y. Deng, K. van der Wal, D. Ravelli, M. Nuño, M. Fagnoni, D. Guthrie, Y. Sun and T. Noël, *Science*, 2020, **369**, 92–96; (f) A. Pulcinella, D. Mazzarella and T. Noël, *Chem. Commun.*, 2021, **57**, 9956–9967; (g) G. Laudadio, S. Govaerts, Y. Wang, D. Ravelli, H. Koolman, M. Fagnoni, S. Djuric and T. Noël, *Angew. Chem., Int. Ed.*, 2018, **57**, 4078–4082.
- 32 (a) D. Cambié, C. Bottecchia, N. J. W. Straathof, V. Hessel and T. Noël, *Chem. Rev.*, 2016, **116**, 10276–10341; (b) C. Sambigiato and T. Noël, *Trends Chem.*, 2020, **2**, 92–106; (c) M. Baumann, T. S. Moody, M. Smyth and S. Wharry, *Org. Process Res. Dev.*, 2020, **24**, 1802–1813; (d) V. Klöpfer, R. Eckl, J. Floß, P. M. C. Roth, O. Reiser and J. P. Barham, *Green Chem.*, 2021, **23**, 6366–6372.
- 33 (a) J. A. Ripper, E. R. T. Tiekink and P. J. Scammells, *Bioorg. Med. Chem. Lett.*, 2001, **11**, 443–445; (b) Y. Chen, G. Glotz, D. Cantillo and C. O. Kappe, *Chem.–Eur. J.*, 2020, **26**, 2973–2979.
- 34 Y. Pan, S. Wang, C. W. Kee, E. Dubuisson, Y. Yang, K. P. Loh and C. H. Tan, *Green Chem.*, 2011, **13**, 3341–3344.
- 35 (a) Y. Zhang, D. Riemer, W. Schilling, J. Kollmann and S. Das, *ACS Catal.*, 2018, **8**, 6659–6664; for a related transformation of ureas, see: (b) H. Wang, Y. Man, K. Wang, X. Wan, L. Tong, N. Li and B. Tang, *Chem. Commun.*, 2018, **54**, 10989–10992.
- 36 J. Santamaria, *Pure Appl. Chem.*, 1995, **67**, 141–147.
- 37 J. Santamaria, R. Ouchabane and J. Rigaudy, *Tetrahedron Lett.*, 1989, **30**, 3977–3980.
- 38 F. Glöckhofer, A. J. Morawietz, B. Stöger, M. M. Unterlass and J. Fröhlich, *ACS Omega*, 2017, **2**, 1594–1600.
- 39 M. F. Acquavella, M. E. Evans, S. W. Farraher, C. J. Nevoret and C. J. Abelt, *J. Org. Chem.*, 1994, **59**, 2894–2897.
- 40 (a) M. L. Crossley, *J. Am. Chem. Soc.*, 1915, **37**, 2178–2181; (b) E. Schwenk, *Angew. Chem.*, 1931, **44**, 912–913.
- 41 T. Hinoue, Y. Shigenoi, M. Sugino, Y. Mizobe, I. Hisaki, M. Miyata and N. Tohnai, *Chem.–Eur. J.*, 2012, **18**, 4634–4643.
- 42 Y. Mizobe, T. Hinoue, A. Yamamoto, I. Hisaki, M. Miyata, Y. Hasegawa and N. Tohnai, *Chem.–Eur. J.*, 2009, **15**, 8175–8184.
- 43 Theoretical solubilities were gauged using calculated log *P* and total polar surface area. Calculations were made using: Molinspiration Cheminformatics, Slovensky Grob, Slovakia, <https://www.molinspiration.com/>. for further details, see ESI.
- 44 (a) T. Shida, *Electronic Absorption Spectra of Radical Ions. Physical Sciences Data*, Elsevier, 1988, vol. 34; (b) D. T. Breslin and M. A. Fox, *J. Phys. Chem.*, 1994, **98**, 408–411.
- 45 (a) J. M. Achord and C. L. Hussey, *Anal. Chem.*, 1980, **52**, 601–602; (b) D. Dvoranová, Z. Barbieriková and V. Brezová, *Molecules*, 2014, **19**, 17279–17304.
- 46 R. Takeda, S. Y. Ryu, J. H. Park and K. Nakanishi, *Tetrahedron*, 1990, **46**, 5533–5542.
- 47 T. Karatsu, K. Kanayama, M. Takahashi, N. Ishigohoka, K. Fukui and A. Kitamura, *Heteroat. Chem.*, 2001, **12**, 269–275.
- 48 Z. Y. Chan, P. Krishnan, S. M. Modaresi, L. W. Hii, C. W. Mai, W. M. Lim, C. O. Leong, Y. Y. Low, S. K. Wong, K. T. Yong, A. Z. X. Leong, M. K. Lee, K. N. Ting and K. H. Lim, *J. Nat. Prod.*, 2021, **84**, 2272–2282.
- 49 (a) P. J. Dunn, *Org. Process Res. Dev.*, 2005, **9**, 88–97; (b) P. Lees and F. Shojaei Aliabadi, *Int. J. Antimicrob. Agents*, 2002, **19**, 269–284.



- 50 J. Castellanos-Soriano, J. C. Herrera-Luna, D. Díaz Díaz, M. C. Jiménez and R. Pérez-Ruiz, *Org. Chem. Front.*, 2020, 7, 1709–1716.
- 51 M. Neumeier, D. Sampedro, M. Májek, V. A. D. O'Shea, A. Jacobi von Wangelin and R. Pérez-Ruiz, *Chem.–Eur. J.*, 2018, 24, 105–108.
- 52 (a) J. P. Barham and B. König, *Angew. Chem., Int. Ed.*, 2020, 59, 11732–11747; (b) H. Kim, H. Kim, T. H. Lambert and S. Lin, *J. Am. Chem. Soc.*, 2020, 142, 2087–2092; (c) X. Tian, T. A. Karl, S. Reiter, S. Yakubov, R. de Vivie-Riedle, B. König and J. P. Barham, *Angew. Chem., Int. Ed.*, 2021, 60, 20817–20825; (d) A. F. Chmiel, O. P. Williams, C. P. Chernowsky, C. S. Yeung and Z. K. Wickens, *J. Am. Chem. Soc.*, 2021, 143, 10882–10889.
- 53 For representative reviews on radical ion photocatalyst reactions and physical properties, see: S. Wu, J. Kaur, T. A. Karl, X. Tian and J. P. Barham, *Angew. Chem., Int. Ed.*, 2021, DOI: 10.1002/anie.202107811 and ref. 44b.
- 54 (a) D. B. Vogt, C. P. Seath, H. Wang and N. T. Jui, *J. Am. Chem. Soc.*, 2019, 141, 13203–13211; (b) I. A. MacKenzie, L. Wang, N. P. R. Onuska, O. F. Williams, K. Begam, A. M. Moran, B. D. Dunietz and D. A. Nicewicz, *Nature*, 2020, 580, 76–80; (c) J. P. Cole, D.-F. Chen, M. Kudisch, R. M. Pearson, C.-H. Lim and G. M. Miyake, *J. Am. Chem. Soc.*, 2020, 142, 13573–13581; (d) C. M. Hendy, G. C. Smith, Z. Xu, T. Lian and N. T. Jui, *J. Am. Chem. Soc.*, 2021, 143, 8987–8992.
- 55 E. Doni, B. Mondal, S. O'Sullivan, T. Tuttle and J. A. Murphy, *J. Am. Chem. Soc.*, 2013, 135, 10934–10937.
- 56 (a) S. P. Pitre, C. D. McTiernan and J. C. Scaiano, *Acc. Chem. Res.*, 2016, 49, 1320–1330; (b) D. Rehm and A. Weller, *Ber. Bunsen. Phys. Chem.*, 1969, 73, 834–839; (c) D. Rehm and A. Weller, *Isr. J. Chem.*, 1970, 8, 259–271; (d) For a general review about the importance of mechanistic studies in photocatalysis, see: L. Buzzetti, G. E. M. Crisenza and P. Melchiorre, *Angew. Chem., Int. Ed.*, 2019, 58, 3730–3747.
- 57 R. F. Bartholomew and R. S. Davidson, *J. Chem. Soc. C*, 1971, 2347–2351.
- 58 In MeCN, the diffusion-controlled rate constant is expected to be $ca. 2 \times 10^{10} \text{ M}^{-1} \text{ s}^{-1}$ at rt. See: S. Blanc, T. Pigot, C. Cugnet, R. Brown and S. Lacombe, *Phys. Chem. Chem. Phys.*, 2010, 12, 11280–11290.
- 59 Bimolecular quenching of DCA by photoinduced electron transfer is known to proceed beyond the diffusion limit in MeCN. Rates as high as $10^{12} \text{ M}^{-1} \text{ s}^{-1}$ can be still rationalized within Marcus theory. See: A. Rosspeintner, G. Angulo and E. Vauthey, *J. Am. Chem. Soc.*, 2014, 136, 2026–2032.
- 60 For recent reviews on the effect of aggregation on photoredox properties see: (a) A. Bhattacharyya, S. de Sarkar and A. Das, *ACS Catal.*, 2021, 11, 710–733; (b) D. Bialas, E. Kirchner, M. Röhr and F. Würthner, *J. Am. Chem. Soc.*, 2021, 143, 4500–4518.
- 61 (a) DCA molecules are known to π -stack, a phenomenon that is receiving attention in photoredox catalysis giving rise to self-assembled organic dyes with enhanced redox properties (see ref. 60). The XRD of DCAS clearly shows a disruption of π -stacking due to a large π -plane distance of 13.60 Å. While we recognize aggregation can differ in solution and solid-state, our DFT calculated radius of DCAS using an implicit solvation model gave $ca. 6.7 \text{ Å}$ (thus 13.4 Å between two 'spherical' molecules), see ESI†. Therefore, bulky substituents inhibit π -stacking aggregation of solvated DCAS. Moreover, fluorescence lifetime decay profiles of the two catalysts indicated a different aggregation for DCAS. Consistent with literature: ref. 58; (b) A. F. Olea, D. R. Worrall, F. Wilkinson, S. L. Williams and A. A. Abdel-Shafi, *Phys. Chem. Chem. Phys.*, 2002, 4, 161–167, we observed monoexponential decay profiles for DCA (see ESI†). For DCAS (alone, under Ar), a multiexponential decay was observed indicating a static self-quenching that points to a different kind of aggregation in solution vs. DCA. We recognize the possibility the electron transfer event between $^1\text{DCAS}^*$ and amines occurs at the Marcus inverted region, accounting for the unintuitive relationship between the SET driving force (ΔG_{SET}) and kinetics (k_{q}). Overall, we postulate the Marcus inverted region and different aggregation pattern may work together to suppress reductive quenching in the case of $^1\text{DCAS}^*$.
- 62 Singlet oxygen generation via $E_{\text{n}}T$ from dicyanoanthracenes is known, see: (a) C. Schweitzer and R. Schmidt, *Chem. Rev.*, 2003, 103, 1685–1758. It was reported that singlet oxygen can be produced from both singlet and triplet excited states of dicyanoanthracenes, see: (b) R. C. Kanner and C. S. Foote, *J. Am. Chem. Soc.*, 1992, 114, 678–681.
- 63 (a) X. Han, R. A. Bourne, M. Poliakoff and M. W. George, *Chem. Sci.*, 2011, 2, 1059–1067; (b) T. B. Truong and J. Santamaria, *J. Chem. Soc., Perkin Trans. 2*, 1987, 1–5; (c) K. Zhang, Z. Vobecka, K. Tauer, M. Antonietti and F. Vilela, *Chem. Commun.*, 2013, 49, 11158–11160.
- 64 (a) E. Baciocchi, T. Del Giacco and A. Lapi, *Org. Lett.*, 2004, 6, 4791–4794; (b) S. K. Silverman and C. S. Foote, *J. Am. Chem. Soc.*, 1991, 113, 7672–7675.
- 65 The fact that trialkylamines themselves can act as physical quenchers of $^1\text{O}_2$ supports the need for sufficient $[\text{O}_2]$ to counteract this toward productive reactions, thus further justifying the use of continuous flow.
- 66 (a) J. Xiao, Z. Yin, B. Yang, Y. Liu, L. Ji, J. Guo, L. Huang, X. Liu, Q. Yan, H. Zhang and Q. Zhang, *Nanoscale*, 2011, 3, 4720–4723; (b) T. Imagawa, M. Nakamoto, R. Shang, Y. Adachi, J. Ohshita, N. Tsunoji and Y. Yamamoto, *Chem. Lett.*, 2020, 49, 1022–1025; (c) C. Janiak, *J. Chem. Soc., Dalton Trans.*, 2000, 3885–3896.
- 67 E. Alfonzo and A. B. Beeler, *Chem. Sci.*, 2019, 10, 7746–7754.
- 68 A. P. Darmanyany, W. S. Jenks and P. Jardon, *J. Phys. Chem. A*, 1998, 102, 7420–7426.
- 69 I. Saito, T. Matsuura and K. Inoue, *J. Am. Chem. Soc.*, 1981, 103, 188–190.
- 70 Catalytically-generated $^1\text{O}_2$ finds utility in LSF modification of many natural products containing alkene and diene moieties. Far fewer examples are known for amines due to their physical quenching of $^1\text{O}_2$, see: A. A. Ghogare and A. Greer, *Chem. Rev.*, 2016, 116, 9994–10034. We envisage



the method herein may inspire further development of catalytically generated $^1\text{O}_2$ as an LSF strategy for amines.

71 (a) M. Rueping, C. Vila, A. Szadkowska, R. M. Koenigs and J. Fronert, *ACS Catal.*, 2012, 2, 2810–2815; (b)

D. B. Ushakov, M. B. Plutschack, K. Gilmore and P. H. Seeberger, *Chem.–Eur. J.*, 2015, 21, 6528–6534; (c) X. Lang, W. Ma, Y. Zhao, C. Chen, H. Ji and J. Zhao, *Chem.–Eur. J.*, 2012, 18, 2624–2631.

